Preferred citation: X. Thibault, Y. Chave, J-M. Serra-Tosio and J-F. Bloch. Permeability Measurements of Press Felts. In **The science of papermaking**, *Trans. of the XIIth Fund. Res. Symp. Oxford, 2001*, (C.F. Baker, ed.), pp 947–974, FRC, Manchester, 2018. DOI: 10.15376/frc.2001.2.947.

PERMEABILITY MEASUREMENTS OF PRESS FELTS

X. Thibault, Y. Chave, J-M. Serra-Tosio and J-F. Bloch

Laboratoire Génie des Procédés Papetiers
(LGP2/ EFPG/ CTP/ CNRS UMR 5518)
BP 65, 38402 Saint-Martin-d'Hères Cedex
Jean-Francis.Bloch@efpg.inpg.fr

INTRODUCTION

The main aim of the successive unit operations of the papermaking process is to remove water from the fibrous web. Water is removed mechanically during the forming and pressing operations. The sheet is then dried in the dryer section further along the paper machine. Classically, the necessary energy for evaporating water by drying is six times higher than the energy required to remove the same quantity of water by pressing. Consequently the more water is removed by the forming and pressing operations, the lower the production costs are. Therefore, an efficient press section has a very definite influence on the whole economy of a paper mill.

In this paper, the main developments of the press section in the last century are briefly presented. The evolution of pressing theory and areas of research are discussed. In a second part, the theoretical and experimental backgrounds of flow resistance in a press felt are given. Then, the built experimental device is described and finally results of transverse and in-plane permeability measurements are analysed.

LITERATURE

Pressing history

Most of the earliest paper machine press sections were equipped with plain presses: two smooth rolls pressed the paper sheet supported by a felt (Figure 1). The main drawback of this technology is that, as the paper machine production speed increases, the hydraulic pressure inside the press nip rises dramatically and crushing of the paper sheet may occur. To overcome this drawback, the water flow length in the press nip had to be decreased. Grooved and blind drilled presses were therefore major advances. In the sixties, the fabric press and then the suction press were developed. Later, the extended nip and high impulse pressing concepts were designed, leading to the development of modern shoe press. The latest development in pressing technology is the impulse pressing press (or often called impulse drying), which combines pressing and heating at high temperature. With this process the distinction between pressing and drying is going to blur [1]. Some examples of this technology are described through experimental trials conducted in the Swedish Pulp and Paper Research Institute (STFI) [2] or in the Institute for Paper and Science Technology (IPST) [3].

In order to improve dewatering in press section, two kinds of solutions exist. One is to radically change press design, and build a new press section for example with a higher mechanical impulse (see Figure 1), i.e. a longer nip or a higher load.

$$I = \int_{\Delta t} \sigma(t)dt = \overline{\sigma} \cdot \Delta t$$

σ : total pressure in the nip.

$\overline{\sigma}$: average total pressure.

t : time variable.

Δt : nip length.

I : mechanical impulse

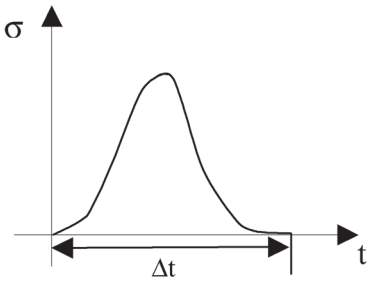

Figure 1 Evaluation of the press impulse.

The other solution is to add new devices or modify elements in the press section: adding steam boxes, optimising the rolls or the press closing. Examples of press optimisation were described by Wheeldon and Green [4]. They showed that increasing the nip load was not always the best alternative but changing the felt could be more profitable. In the case of press clothing, the main characteristics of the felt (compressibility, uniformity of load distribution, flow resistance of felt structure and life expectancy) have to be well described and understood. The present work deals with the determination of permeability (inverse of the flow resistance) in strained felts to satisfy the need of felt manufacturers to characterise their product.

Theoretical background

Numerous studies have been made on pressing this last forty years. Wahlström provided a useful basis for qualitative models of wet pressing. He postulated, on one hand, the compressive stress has to be balanced in the press nip by the hydraulic pressure and the structural stress. On the other hand, the hydraulic pressure and the water flow start rising when the web becomes saturated [5,6]. His theory has been widely accepted and has been since qualitatively improved. First of all, a more precise flow description in the nip is made by Asklöf [7] and next Nilsson and Larsson [8]. The rewetting phenomenon after the nip, which is controlled by the capillary forces, was examined by Wahlström et al. [9]. A model taking into account the inertial effects of water entering and leaving the nip, and also the dynamic shrinkage of the press nip because of the increasing rigidity of the roll clothing with faster solicitations, was proposed by Gudehus [10]. If the explanations proposed by these authors represent major advances in pressing theory, they did not allow any prediction of press efficiency. In his work on pressing simulation, Roux [11] underlined that the validation of a pressing model is very difficult, if not impossible, due to the lack of measurements in press sections. Nowadays, some quantitative pressing models are more effective owing to the use of laboratory pilot paper machines [12]. The major part of these models is based on phenomenological approaches of the wet pressed web and therefore there is an obvious need of a database for paper and felt characteristics. In this paper only the permeability of felt will be considered.

The Reynolds number is commonly used to study the flow through a pipe or a porous medium. This dimensionless number is defined as the ratio of the inertial to viscous terms of the Navier Stokes equation. If this number is small, the flow is laminar (creep flow). On the contrary, if the number is high, the flow is turbulent. Classically, water flow in the press nip is characterised

by a small Reynolds number. Consequently, the water flow may be considered as laminar.

The analytical approach of the flow inside a porous media is very difficult because of the structure complexity. Early in last century, experimental studies lead to empirical laws relying the seepage velocity of the fluid relatively to the porous media and the pressure drop. When the flow through a rigid porous medium is laminar, the generalised to three spatial dimensions Darcy's equation (Equation 1) may be applied [13].

$$\mathbf{v} = -\frac{\overline{\mathrm{K}}}{\mu}\,\mathbf{grad}(\mathrm{P}) \tag{1}$$

In this equation, **v** is the seepage velocity vector or volumetric flux density (in $m.s^{-1}$), P the pressure field (in Pa), μ the fluid viscosity (in s^{-1}) and $\overline{\mathbf{K}}$ the permeability tensor (in m^2).

To rely the permeability to structural parameters, several theoretical and experimental studies have been carried out. Among them the well-known work of Carman [14] leads to the following empirical formula (Equation 2):

$$\mathrm{K} = \frac{\varepsilon^3}{\mathrm{k_o}\tau^2\mathrm{S_v^2}} \tag{2}$$

where ε is the porosity, S_v the volumic specific surface of the porous medium (in m^2/m^3), τ the tortuosity and k_o is a constant called the Kozeny–Carman constant. The porosity is the ratio of the void volume to effective total volume of the porous web. The tortuosity is the ratio of the average length of the fluid flow inside the web to the apparent length of the flow. The volumic specific surface is the ratio of the wettable surface to the volume of the porous web. This relation was established for a wide range of granular and fibrous media with porosity from 0.286 to 0.574 [15]. However, the Kozeny–Carman formula does not take into account the direction of the flow through the porous structure. Rahli [16] proposed a literature review of empirical or theoretical works on variation of Kozeny–Carman constant with porosity. In his study of random orientated stack of monodisperse fibres, he found that the permeability-porosity relationship fitted very well with an exponential function inspired from Kyan work [17]. So in the presented work, Kozeny–Carman and based-10 exponential models (see experimental results paragraph) are compared in the experimental results. The main asset of based-10 exponential function on exponential one is that the order of magnitude is quite easily found. In the last two described

works, the porosity is evaluated from the basis weight. In our study, the following notation is used for porosity evaluation: basis weight w (kg/m^2), the density of the fibres ρ_f (kg/m^3); and the thickness e (m). The classical relationship is:

$$\varepsilon = 1 - \frac{w}{e \cdot \rho_f} \tag{3}$$

In the context of this study, the porous media is a felt and its porosity during pressing is often lower than the porosity range of Kozeny–Carman law. Therefore the applicability of this law is not obvious.

Biot [18] and Auriault [19] discussed and proved the validity of the Darcy's law for non-saturated deformable porous media. It remains from their works that this law is also applicable in the case of linear elastic behaviour with small deformation and immiscible two-phase flow. Auriault [20] generalized the homogenization techniques of locally periodic porous media to random ones. Homogenized approach is the description of the continuous media equivalent to the complex description of the media with all the microscopic heterogeneities. The main assumption for applying this method is a good separation of the microscopic and the macroscopic scales of the problem. Hence, the permeability tensor depends only of the geometrical characteristics of the structure and if this geometry is known direct evaluation of the permeability is possible.

EXPERIMENTAL REVIEW

Only a few experimental studies on press felt permeability have been published. Macklem [21] studied the flow resistance of wool felts in transverse and lateral directions. He showed that Kozeny–Carman equation could describe the flow through press felts. However the Kozeny–Carman constant, k_o would not be the same for transverse or lateral flows. Kershaw [22] studied the flow resistance of felts in three directions. The in-plane one was roughly isotrope for all tested felts. In these works, the lateral permeability was higher or equal to the transverse one. Ballard [23] studied the permeability of 100% synthetics felts. He found that felt with monofilament base offered superior permeability under load than other type of tested felts. Chevallier [24] pointed out that felt permeability is tension stress dependent. All of these authors used a unidirectional flow device to measure the in-plane permeability. To measure transverse permeability, the flow direction is usually in the direction orthogonal to the felt plane. A linear relationship between the

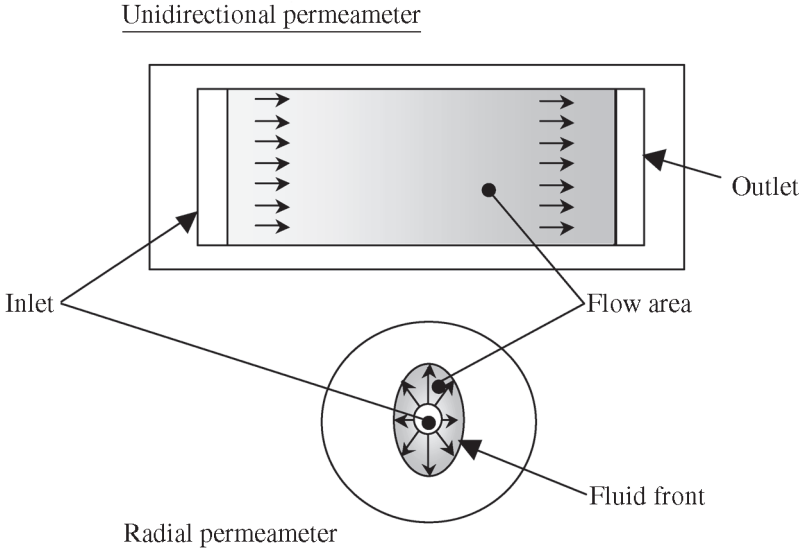

Figure 2 Schema illustrating the principles of unidirectional and radial permeameters.

pressure gradient and the seepage velocity is found in each experimental work that may lead to the permeability computation. Nowadays, industrial felt permeability measurement equipment exists [25]. These permeability measurements consist in imposing the pressure drop and measure the flow rate through a known section. However, it can be used only on non-strained felt.

Nevertheless, in the textile research field (fibre reinforcement), many experimental studies of the in-plane permeability of woven and non-woven textiles were done using unidirectional or radial flow devices (Figure 2). Radial flow consists in injecting a fluid in the centre of the saturated or unsaturated sample and studies the progress of the flow front. Usually, this method allows the determination of the principal axes of the permeability tensor. Parnas [26,27], compared the measurement of flow resistance with both device. He found close results for different woven glass materials which porosities ranged from 45% to 80%. Young [28], studied the average in-plane permeability–compression dependence with the radial flow method. His results showed non-linearity attributed to the woven web deformations. Furthemore, permeability as a function of porosity fits very well with an exponential relationship. Lekakou [29] compared the measurement of the average in-plane permeability using unidirectional and radial techniques.

Permeability values obtained with the unidirectional method were one order of magnitude higher than with the values measured with the other method. In both cases, the decrease of permeability with the decrease of porosity was verified with Kozeny–Carman law. However, in the case of the radial flow experiments, if the progression of the flow front was well described with the Darcy's law, the permeability values were paradoxically dependent of the injected flow rate. Gebart [30] compared the radial and the unidirectional flow methods. He showed that both method results are similar. Nevertheless, the radial flow techniques may have large error if the mold is not stiff enough (deformation of the measurement cell). He proposed a multi-cavity parallel flow apparatus in order to improve the unidirectional flow technique. Experimental results with this equipment showed excellent repeatability [31] and reproducibility [32] with woven and non-woven glass fiber. This repeatability is limited by the natural variance of the tested media. Lundström noticed that the anisotropy increase when the porosity decrease. The porosity range was from 70% to 50%, permeability range from 150 μm^2 to 17 μm^2 and the anisotropy ratio from 1 to 10. The author found small differences in permeability value when using saturated and non saturated flow. In an error analysis, he showed that when the anisotropy ratio increase, so the error does. In order to improve the measurements, the shape of the unidirectional permeability cell has to verify that the flow length–flow wide ratio is higher than the anisotropy ratio.

DESCRIPTION OF THE NEW EXPERIMENTAL DEVICE.

The new experimental device (Figure 3) imposes a flow either perpendicular to the felt plane, or in an imposed in-plane direction in order to measure the Darcian permeability in that direction. The ultimate aim is to be able to perform easy, on-machine measurements on a press felt during machine stops. This objective, conjugated to the requirement of avoiding adventitious felt strains, led to the decision not to use any sealing in the felt plane. Thus lateral leakage may exist. A guard area is therefore used in order to measure only the flow that is not influenced by this potential leakage.

Case of the transverse permeability

Description of the experimental device

In the case of transverse permeability measurement, the flow is measured in a circular area of 57 mm large. The total measurement cell diameter is 120 mm.

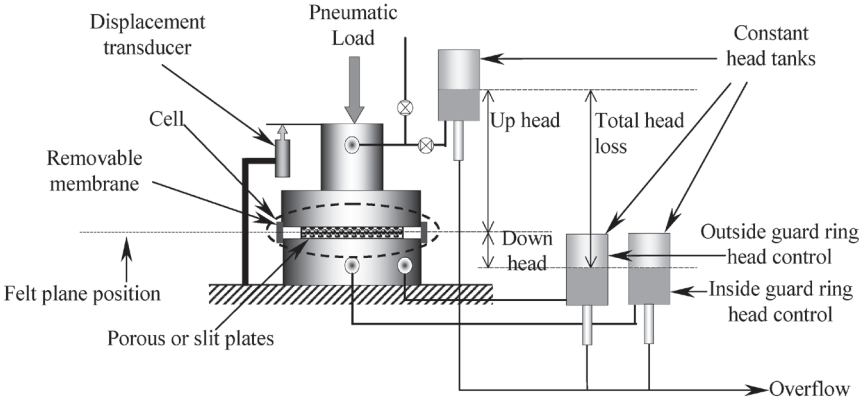

Figure 3 Schematic diagram of permeameter equipment.

Porous plates are used in order to homogenize the flow and the imposed stress. For the pressure drops from 0 to 15 kPa, three constant head tanks create the flow. The two downstream ones are always at the same height (see Figure 3). The error on pressure drop measurements is about 20 Pa.

A pneumatic jack can load mechanically the permeameter cell (see Figure 3) up to 5.5 MPa. A displacement transducer (LVdT) measures the position of the upper part with an accuracy of 10 μm. An external stress (tension in one direction in the plane of the felt) may be applied to the felt during measurements.

Weighing and timing with measurements accuracy of 5 g and 1 s respectively, are used to calculate the flow rate. The temperature, T (°C) is measured with an alcohol thermometer. The accuracy is about 0.5°C. The viscosity, μ (Pa.s^{-1}) is evaluated with the following Bingham formula in which the temperature is in degree Celsius:

$$\mu = \frac{0.1}{(2.1482 \cdot ((T - 8.8432) + (8078.4 + (T - 8.435)^2)^{1/2}) - 120)} \quad (4)$$

An example of numerical simulation of flow through both porous disks and a felt is presented in Figure 4. The numerical problem is considered to be axisymmetric. On the upper part, the pressure condition is set to 1.18 bar (i.e., 1 atmosphere and 80 cm column of water). Under the down part, pressure is imposed to be 1.08 bar (i.e. one atmosphere minus 20 cm column of water). Outside pressure condition is set to 1.1 bar (1 atmosphere). The velocity field reveals that the outside pressure drop does not influence the flow

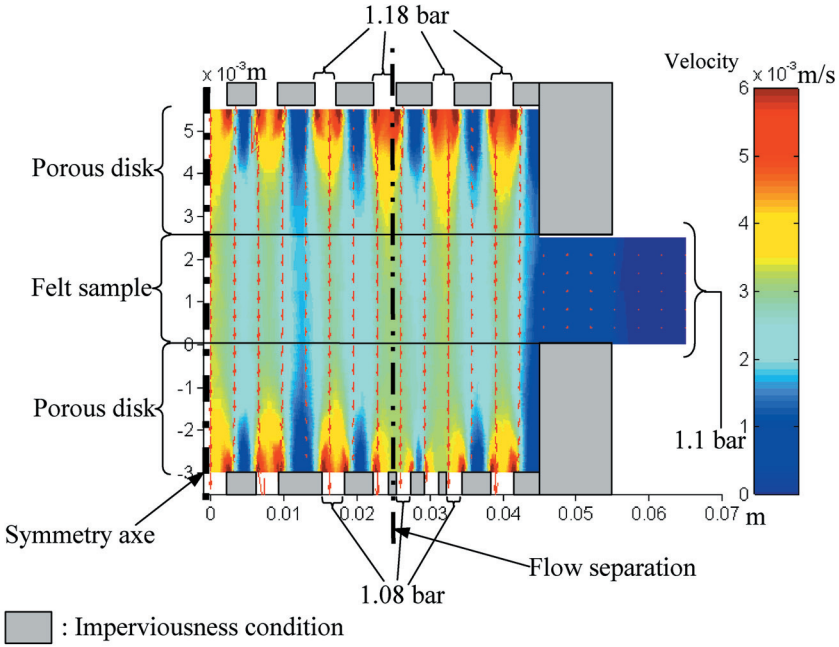

Figure 4 Simulation of the flow in a half cross section of the transverse permeametre. Arrows represent the velocity field.

in the central zone. More details concerning the method of design are presented in [33,34].

Experimental procedures

Felt samples are saturated in water 24 hours before the experiments. Before any measurement, the cell is compressed without sample in order to determine the mechanical deformation of the experimental equipment for imposed stresses.

When measuring transverse permeability, the device is first calibrated. This step of calibration consists in the evaluation of the pressure drop–flow rate relationship of the apparatus without a felt sample. No variation of the porous disks permeability was noticed whatever the loading stresses were. Afterwards, a felt sample is introduced into the cell, which is loaded to a chosen stress level. After the felt creep (15 or 20 minutes), the pressure drop–flow rate relationship is evaluated. For each measurement of flow rate, the

temperature is measured. The Darcian permeability is then deduced using the calibration. The linearity, and thus the validity of Darcy's law, is checked for all measurements. The pressure drop (ΔP) versus modified flow rate (μQ) relationship is obtained with a least square regression method. Thus, temperature variations, that may occur for successive measurements, are taken into account. The uncertainty range is computed for each permeability evaluation. Details of this calculation are shown in Annexe I.

Case of the in-plane permeability

Description of the experimental device

In the case of in-plane measurements, slit plates replace porous disks in order to impose an in-plane unidirectional flow. The fluid arrives through two

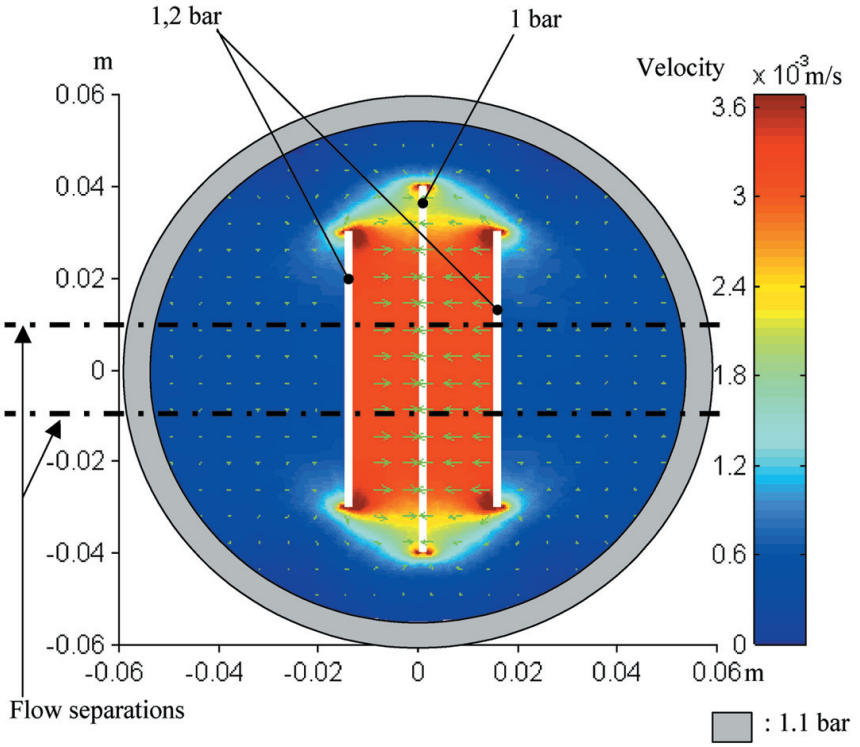

Figure 5 Simulation of the flow in a elevation section of the in-plane permeametre. Arrows represent the velocity field.

parallel slits (inlets) and leaves by a central one (outlet) (see Figure 5). The two upstream inlets are symmetrically positioned in respect of the downstream outlet. An example of flow computation in the felt is shown hereafter in Figure 5. Outside pressure is set to atmospheric condition (1.1 bar). Extern slits pressure is set to 1.2 bar. The central slit one is set to 1 bar. This numerical result shows that the flow is not affected by outside pressure condition in a 30 mm large central zone.

In order to take into account the potential influence of the transverse permeability, the flow was computed in the half cross section perpendicular to the slits (Figure 6). The problem is described as symmetrical respectively to the ordinate axe. The model results show that the flow is mostly horizontal between the slit and leakage of water to the outside is not predominant. Hence, if necessary in-plane measured values may be corrected by the knowledge of the transverse permeability. In this simulation pressure conditions

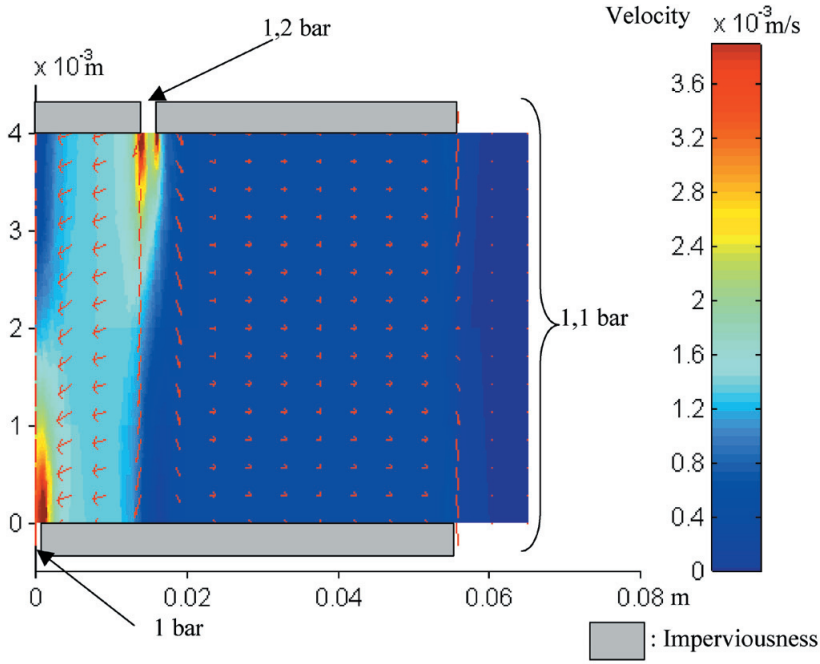

Figure 6 Simulation of the flow in a half cross section of the in-plane permeametre. Arrows represent the velocity field.

are identical to computation boundaries conditions considered in the transversal case.

For the same levels of pressure drop, flow rates are expected smaller than with the transverse permeameter characteristics). Therefore, the used pressure drop ranges from 10 kPa to 250 kPa in order to obtain a measurable flow rate. Current water network is connected instead of the upstream tanks. Electronics and mechanical equipments remain the same as for the transverse permeameter design, except for the upstream pressure, which is measured by an analogical manometer with an accuracy of 5 kPa.

Experimental procedure

The procedure to measure the in-plane permeability in respect of the felt strain is similar to the transverse permeability measurement one, except the first calibration step. Due to large head loss created by the felt sample, there is no need for calibrating the empty device. The detail of the calculation of the uncertainty range on the measurements is shown in Annexe I.

EXPERIMENTAL RESULTS

All performed experiments were run with current water. Preliminary trials were made to test the procedure [33,34]. We focused our attention on the guard ring efficiency, the sample preparation and the representativity of the tested sample. Initial trials were conducted using samples, which were saturated and desaerated, and other, which were only simply saturated. No significant difference was notice. Therefore next experiments were conducted with saturated sample. Some trials were conducted with and without lateral leakage. The results of this set of experiments demonstrate the efficiency of the guard area concept on the lateral boundary of the felt. In the case of transverse permeability, trials had been made with one and two stacked samples taken from a single felt. The results reveal that, the transverse permeability measurements are not affected by the interface between the porous disks and the felt sample. Consequently, the measured permeability values are intrinsic.

Generally, felt samples come from the clipping of felt making. Hence because of the edge effects due to manufacturing, its structure may present important variation (for example variation of basis weight). This could provide permeability variation measurements. Compacting the felt samples before the permeability measurement was not done. Therefore, tested felt are uncompressed felts. The main characteristics values of tested felt sample are summed up in the Table 1.

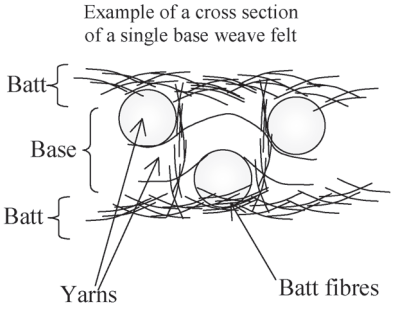

(1) MD: Machine Direction, yarns number X diameters

(2) C.D: Cross Machine Direction.

(3) C.D oriented batt.

Table 1 Tested felt properties.

Sample	Basis Weight	Base	Batt	Base yarns diameter mm	Batt fibres average diameter μm
	kg/m^2				
S-1	1600	890	710	Two base weaves (1) MD 6 × 0.20 (2) CMD 0.30	40
S-2	1350	650	700	Two base weaves MD 4 × 0.20 CMD 0.25	51
S-3	1230	420	810(3)	Single base weave MD 6 × 0.20 CMD 0.40	31

Trials were done to study the evolution of permeability after a few compression cycles. The results of these experiments reveal that, the order of magnitude permeability is not affected by the three successive compressions. Therefore, repeatability could be studied in the first cycle of felt compression. Similar results were found by Chevallier [24]. Nevertheless, he showed that significant permeability decrease appear after 50 cycles of compression to 10 MPa. Other authors, among them Lopez [35] pointed out that the felt property modification with compression cycles highly depends on maximum reached stress.

Permeability depends only on felt structure. Felt porosity is a scalar reflecting the ability of the structure to stock water and it is the easiest structural parameter to get. Thus, permeability (μm^2) data are represented as a function of the porosity for different set of experimental (Figures 7 to 12). In the following figures, the cross under the experimental points represents the uncertainty range of the measurement method. The corresponding experimental data are shown in Annexe II.

In Kozeny–Carman formula (see Equation 2), the volumic specific S_v surface may be expressed in respect of S_m the mass specific volume of the web, ρ_f the density of yarns and fibres, and ε the porosity (Equation 5).

$$S_v = \rho_f S_m (1 - \varepsilon) \tag{5}$$

Hence the Equation 2 may be rewritten:

$$K = \frac{1}{k_o \tau^2 (\rho_f S_m)^2} \cdot \frac{\varepsilon^3}{(1 - \varepsilon)^2} \tag{6}$$

Experimental results are fitted with Kozeny–Carman formula and an exponential regression. In the case of Kozeny–Carman formula, experimental data are fitted with the porosity term (see Equation 6). The tortuosity τ and the mass specific surface S_m are assumed as constant (no strain dependency). In Equation 4, the mass specific surface of the web is considered as the sum of the mass specific surface of the components. The value of the parameter $(k_o \tau^2 \rho_f S_m^2)^{-1}$ is shown in Annexe II. This parameter influences only the vertical position of the fit curve. The slope of the curve is imposed by the porosity term.

Exponential phenomenological model need two parameters (see Equation 7).

$$K = \Lambda \cdot 10^{\Psi \cdot \varepsilon} \tag{7}$$

The parameter Ψ is dimensionless. In the presented figure, Ψ reflects the slope of the fitting curve. The parameter $\Lambda(\mu m^2)$ is the ordinate origin of the fitting curve. Both are summed up in Annexe II.

For each sample of felt, two figures are exposed. The first figure is dedicated to the transverse permeability measurements, the second to the in-plane permeability measurements.

When the porosity decreases from 0.55 to 0.32, the transverse permeability of felt S-1 decreases by one and a half order of magnitude (Figure 7). Both models fit very well with the experimental data.

When the porosity decreases from 0.63 to 0.42, in-plane permeability of felt S-1 decreases by one order of magnitude (Figure 8). In-plane permeability seems to be isotrope. In-plane permeability is 3 or 4 times higher than transverse one.

In the case of felt S-2, transverse permeability remains at the same order of magnitude when porosity decreases from 0.54 to 0.34 (Figure 9). Kozeny–Carman does not fit with the experimental data (Figure 9). The decreased of permeability is less than one predicted by the Kozeny–Carman model. The power fitting is a better model.

The S-2 in-plane permeability decreases by one order when the porosity ranges from 0.54 to 0.28. In-plane permeability is in this case anisotrope. The ratio of permeability values in cross and in machine directions increases from

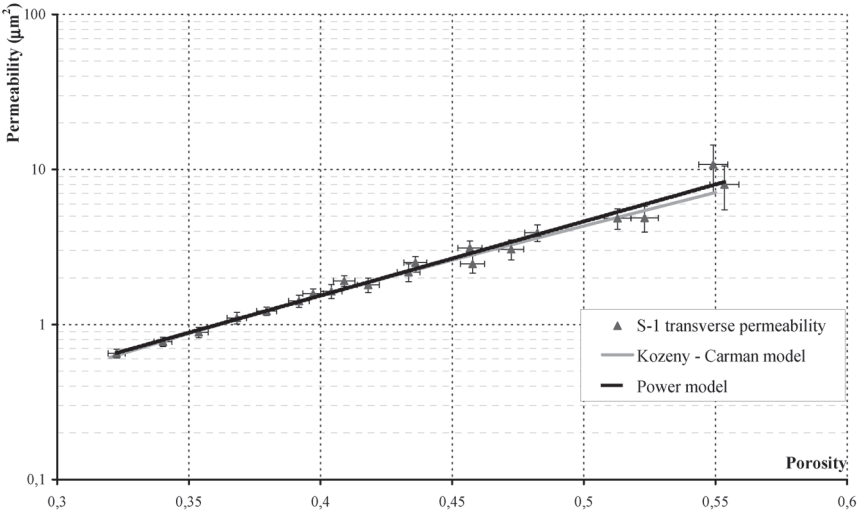

Figure 7 Felt S-1 transverse permeability.

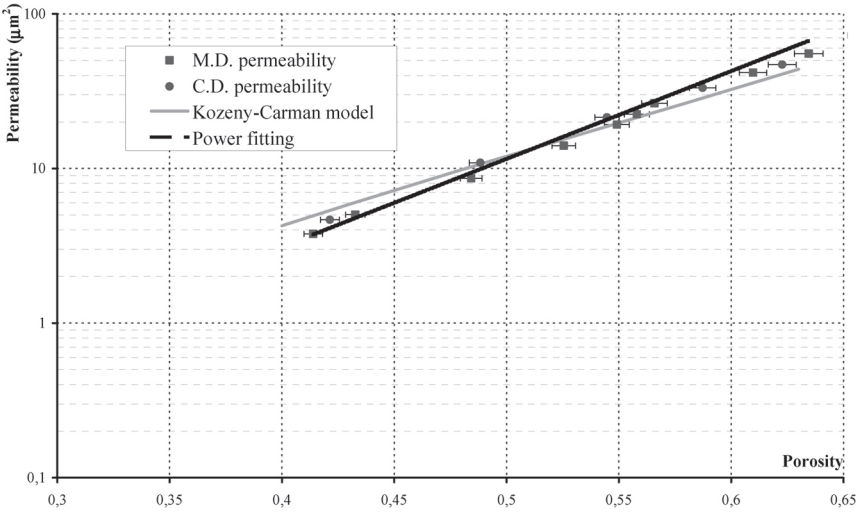

Figure 8 Felt S-1 in-plane permeability.

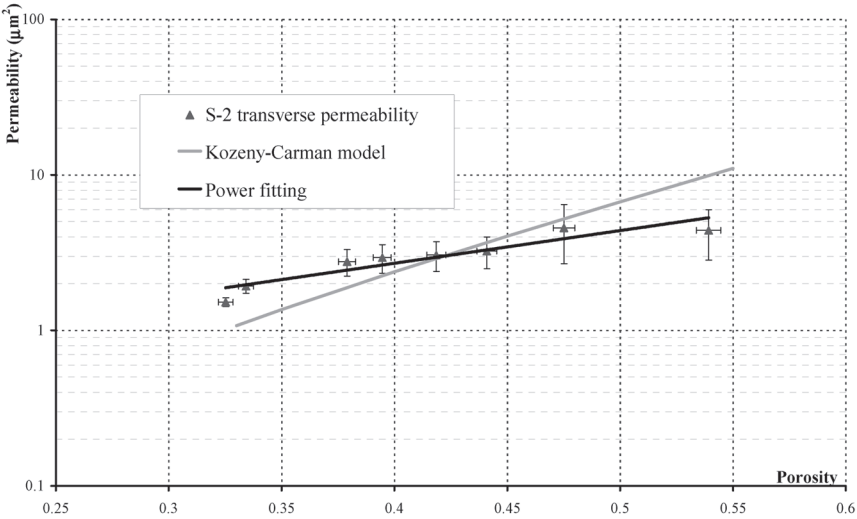

Figure 9 Felt S-2 transverse permeability.

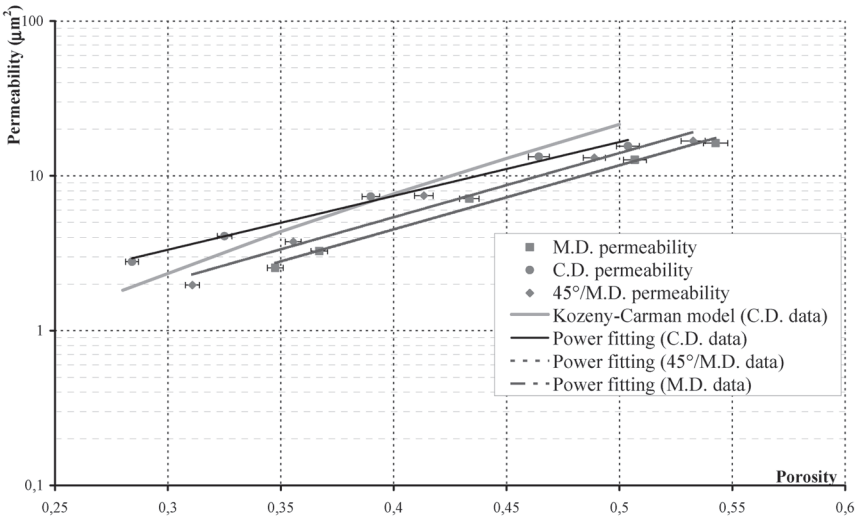

Figure 10 Felt S-2 in-plane permeability.

1.33 to 1.77 in respect of the porosity. The Kozeny–Carman model is not good for the C.D. permeability data (Figure 10) whereas the model is correct for other in-plane direction (M.D. and 45°/M.D.) (not represented in the Figure 10). The decrease of the in-plane permeability (Figure 10) in respect of the porosity is faster than in the case of the transverse one (Figure 9). However even if the gap between transverse and in-plane permeability is decreasing, the last one remains higher.

When S-3 porosity decreased from 0.46 to 0.27, the transverse permeability decreased by one order of magnitude (Figure 11). S-3 transverse permeability behaves like the S-1 one. Both models fit quite well the S-3 transverse data but exponential fitting is better (Figure 11). The results for transverse permeability of S-1 and S-3 samples are similar. This is the more interesting as these felts have very different structures (double base weave for felt S-1 and single base weave for felt S-3, see table 1).

The figure reveals that, during compression, S-2 felt remains quite more permeable in the thickness direction than the two others. The transverse permeability of S-2 has a lighter decrease than with S-1 and S-3 when porosity goes from 0.45 to 0.3. This could mean that during the compression of these felt S-2, no additional flow resistance appears in the thickness direction. In examining the Kozeny–Carman formula, this could reflect that the volumic

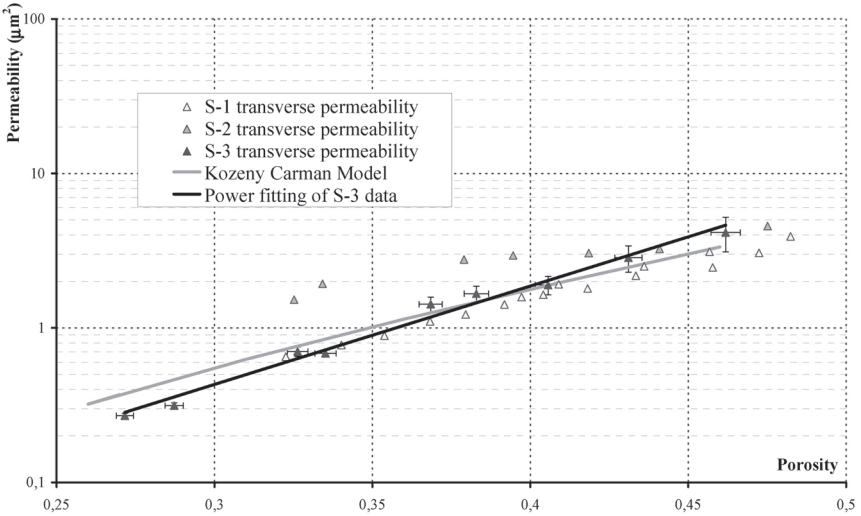

Figure 11 Felt S-3 transverse permeability.

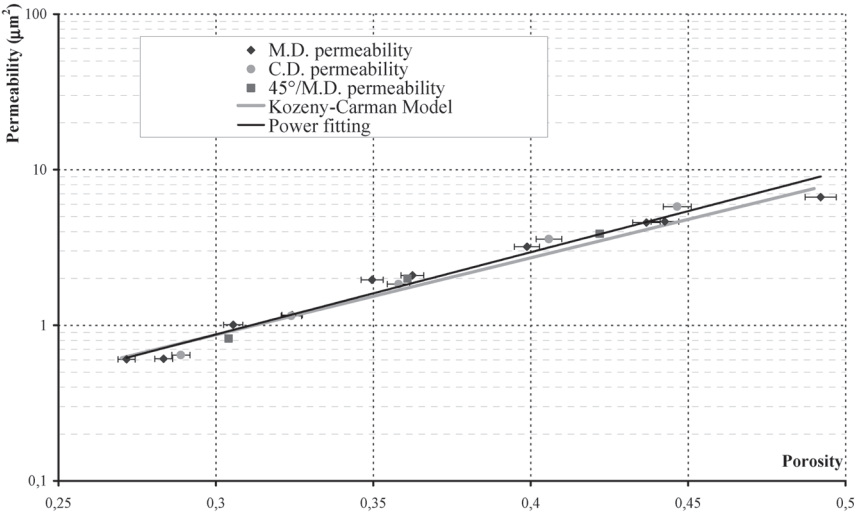

Figure 12 Felt S-3 in-plane permeability.

specific surface and/or the tortuosity decrease when the felt strain decreases.

In the case of S-3 felt in-plane measurements, the results in the Figure 12 are similar in three different in-plane directions. Hence the permeability tensor is isotrope in the plane. The orientation of the paper side batt is in the cross direction. Whereas anisotropic structure induce often anisotropic permeability tensor, felt S-3 presents an isotropic permeability. The in-plane permeability decreases by one order of magnitude when the porosity ranges from 0.49 to 0.27.

CONCLUSION

The presented experimental results are in good agreements with Kershaw permeability tensor description [22]. The in-plane anisotropy remains between 1 and 2 and the in-plane permeability is always higher than the transverse one.

Contrasting with Macklem results [21], Kozeny–Carman model seems not to be an appropriate model for modelling felt permeability. In a phenomenological approach, the exponential model may fit all tested felt better than the Kozeny–Carman formula. Nevertheless, the employed coefficients are not related to the felt structure itself contrary to the Kozeny–Carman parameters.

In order to optimise a given press section, a felt has to be selected. Classically, this choice is made using, among others, knowledge of the unstrained felt transverse permeability. The apparatus described in this paper allows the measurement of felt permeability tensor for different levels of strain. The presented results show that strained felt permeability tensor behaviour might be very different (variation of order of magnitudes, isotrope or anisotrope behaviour). Therefore, the evolution of the felt in strained state may be studied and taken into account in order to optimise the efficiency of a press section. Furthermore, the characterisation of transverse permeability will also improve numerical models of the press.

References

1. Paulapuro, H. and Nordman, L. “Wet pressing : history and future trends”, *Pulp and paper magazine of Canada*, **92**(1): pp 41–50 (1991).
2. Rigdahl, M., *et al*., “Impulse technology on the eurofex machine”. *Tappi J*., peer reviewed paper, **83**(8): pp. 222-230 (2000).
3. Orloff, D. I., Phelan, P. M. and Crouse, J. W., “Impulse drying of board grades: Pilot production trials”, *Tappi J*., peer reviewed paper, **83**(9) (2000).

4. Wheeldon, J. B. and Green, A., "Improving the efficiency of the press section". *Tappi J*., **55**(6): pp. 889–891 (1972).
5. Wahlström, B. J., "A long term study of water removal and moisture distribution on a Newsprint machine press section – Part 2", *Pulp and paper magazine of Canada*, **9**: pp. T418-T451 (1960).
6. Wahlström, B. J., "A long term study of water removal and moisture distribution on a Newsprint machine press section – Part 1", *Pulp and paper magazine of Canada*, **8**: pp. T380-T401 (1960).
7. Asklöf, C. A., *et al*., "Flow conditions in a felt in a plain press nip", *Pulp and paper magazine of Canada*, **6**: pp. T246-T250 (1964).
8. Nilsson, P. and Larsson, K. O., "Paper web performance in a press nip", *Pulp and paper magazine of Canada*, **20**(12): pp. 66–73 (1968).
9. Wahlström, B. J., Johnson, A. and a. co., "Our present understanding of the fundamentals of pressing", *Pulp and paper magazine of Canada*, **70**(19): pp. 76–96 (1969).
10. Gudehus, T., "Stoffentwässerung im Walzenpresspalt (L'essorage de la feuille de papier dans la zone de contact entre les rouleaux de presse)", *Das Papier*, **42**(4, 5, 7) (1988).
11. Roux, J. C., "Modélisation et optimisation du fonctionnement des presses de machines à papier", *APII Fonctionnement des presses de machine à papier*, (3) **23**(1989).
12. Gustafsson, J.-E. and Kaul, V., "A general model of wet pressing", in *Progress in paper physics : a seminar*. Grenoble (2000).
13. Scheidegger, A. E., "The physics through porous media", Third edition, U. o. T. press, Toronto (1974).
14. Carman, P. C., "Fluid flow through granular beds", Trans. Institute chemical engineering, pp. 150–166 (1937).
15. Han, S. T., "Compressibility of fibre mats", *Pulp and paper magazine of Canada*, **T. 1**(5) (1969).
16. Rahli, O., et al., "Etude expérimentale des écoulements darcéens à travers un lits de fibres empilées aléatoirement : influence de la porosité", *Journal de Phyique II*, **11**: p. 1739–1756 (1995).
17. Kyan, C. P., "Flow of single phase through fibrous beds", *Industrial engineer chemical fundamental*, **9**(4) (1970).
18. Biot, M. A., "Mechanics of deformation and acoustic propagation in porous media", *Journal of Applied Physics*, **33**(4): pp. 1482–1498 (1962).
19. Auriault, J.-L., "Nonsaturated deformable porous media: Quasistatics' *Transport in porous media*, **2**: pp. 45–64 (1987).
20. Auriault, J.-L., Cherel, L. and Bonnet, G., "Locally periodic medium and homogenization of random media". *Arch. Mech*, **40**: pp. 529–542 (1988).
21. Macklem, J. E., "A study of the resistance of woven wool felts to liquid flow", *Tappi J*., **44**(8): pp. 535–544 (1961).
22. Kershaw, T. N., "The three dimensions of water flow in press felts", *Tappi J*., **55**(6): pp. 880–887 (1972).
23. Ballard, J. *Press felt characterization*. in *Engineering conference*. 1986. Atlanta.

24. Chevallier, P. and Silvy, J., "La perméabilité directionnelle des feutres de presses humides", La papeterie, (5) (1988).
25. Pikulik, I. I., et al., "A new instrument for measuring the permeability of paper machine clothing" *Tappi J*., **5** (1991).
26. Parnas, R. S. and Salem, A. J., *A comparison of the unidirectional and radial in-plane flow through woven composite reinforcement*. Polymer composite, 1993. **14**(5): pp. 383–394.
27. Parnas, R. S., et al., "Permeability characterisation. Part I: A proposed standard reference fabric for permeability", *Polymer composites* **16**(5): pp. 429–445 (1995).
28. Young, W.-B. and Wu, F., *Permeability measurement of bidirectional woven glass fibers*. Journal of reinforced plastics and composites, **14**(10): pp. 1108–1120 (1995).
29. Lekakou, C., et al., "Measurement techniques and effects on in-plane permeability of woven cloths in resin transfer moulding", *Composites, ed. E. Science. Vol. Part A*. pp. 401–408 (1996).
30. Gebart, R. B. and Lidström, P., "Measurement of in-plane permeability of anisotropic fiber reinforcements", *Polymer composites*, **16**(5): pp. 429–445 (1966).
31. Lundström, S. T., Gebart, R. B. and Sandlund, E., "In-plane permeability measurments on fiber reinforcements by multi-cavity parallel flow technique", *Polymer composites*, **20**(1): pp. 146–154 (1999).
32. Lundström, T. S., et al., "Measurement of the three-dimensional permeability", *Composites, ed. E. Science. Vol. Part A*, pp. 29–43 (2000).
33. Thibault, X. "Permeability measurement of strained felt: Application to paper making process", in *8th World filtration congress*, Brighton (2000).
34. Thibault, X. "Permeability measurement of strained felt: Application to paper making process", in *IDS 2000*. Noordwijkerhout (2000).
35. Lopez, S., "Etude du comportement rhéologique des feutres de machines à papier", in *Génie des procédés*, CPPA, Editor, INPG: Grenoble, p. 392 (1991).

ANNEXE I

Permeability evaluation:

The Darcy's law is $\mathbf{v} = -\frac{\overline{\mathrm{K}}}{\mu}\,\mathbf{grad}(P)$

As presented in this paper, the seepage velocity, v is known owing to the flow rate measurement, Q. The product μQ and the pressure P are fitted with a linear regression (P(μQ)). The result is called A. Hence the transverse permeability of the felt is:

$$\mathrm{K} = \left(\frac{1}{\mathrm{A_o}} - \frac{1}{\mathrm{A_m}}\right) \cdot \frac{\mathrm{e}}{\mathrm{S}}$$

Hereafter, ΔX represents the error or uncertainty range on the variable X. S is the cross section area of the measured flow., e is the thickness of the felt.

In the case of the in-plane permeability, the length uses to calculate the pressure gradient is the distance between slits (ls). Furthemore the surface S depend on the thickness. Thus, the permeability is:

$$K = \left(\frac{1}{A_m}\right) \cdot \frac{e}{S}$$

Error evaluation on measurements

Error on pressure reading:
Reading on a vertical axes : ΔP 1 mm CE or 10 Pa. Thus the uncertainty range on the pressure drop is 20 Pa.
Error on flow rate measurement:
Weighing (mass, M) and timing (time, t): ΔM is 5g and Δt 1 s
Error on temperature reading:
Reading on an alcohol thermometer: 0.5°C
Error on thickness acquisition:
LvdT displacement transducer: Δe is 20μm

Error induced by preliminary data transformation

Error on flow rate evaluation:

$$Q = \frac{M}{t} \Rightarrow \frac{\Delta Q}{Q} = \frac{\Delta M}{M} + \frac{\Delta t}{t}$$

Error on the evaluation of the viscosity:
Bingham formula:

$$\mu = \frac{0.1}{(2.1482 \cdot ((T - 8.8432) + (8078.4 + (T - 8.435)^2)^{1/2}) - 120)}$$

So the derivation of this function is

$$\frac{d\mu}{dT} = 0.1 \cdot \left| \frac{2.1482 \cdot (1 + (T - 8.435)(8078.4 + (T - 8.435)^2)^{-1/2})}{(2.1482 \cdot ((T - 8.8432) + (8078.4 + (T - 8.435)^2)^{1/2}) - 120)^2} \right|$$

The error range on viscosity relatively to the temperature is:

$$\Delta\mu = 0.1 \cdot \left| \frac{2.1482 \cdot (1 + (T - 8.435)(8078.4 + (T - 8.435)^2)^{-1/2})}{(2.1482 \cdot ((T - 8.8432) + (8078.4 + (T - 8.435)^2)^{1/2}) - 120)^2} \right| \Delta T$$

$$\boxed{\Delta\mu = 10\mu^2 \cdot |2.1482 \cdot (1 + (T - 8.435)(8078.4 + (T - 8.435)^2)^{-1/2})| \Delta T}$$

Error on the least square method
The relationship between μQ and P is fitted.

$$S_{qq} = \sum (\mu Q - \overline{\mu Q})^2 \qquad S_{pq} = \sum (\mu Q - \overline{\mu Q})^2 (P - \overline{P}) \qquad A = \frac{S_{pq}}{S_{qq}}$$

The differential of A is:

$$dA = \frac{\partial}{\partial P}\left(\frac{S_{pq}}{S_{qq}}\right) dP + \frac{\partial}{\partial Q}\left(\frac{S_{pq}}{S_{qq}}\right) dQ + \frac{\partial}{\partial \mu}\left(\frac{S_{pq}}{S_{qq}}\right) d\mu$$

$$dA = \frac{1}{S_{qq}} \frac{\partial}{\partial P}(S_{pq}) dP + \frac{S_{qq}\frac{\partial}{\partial Q} S_{pq} - S_{pq}\frac{\partial}{\partial Q} S_{qq}}{S_{qq}^2} dQ + \frac{S_{qq}\frac{\partial}{\partial \mu} S_{pq} - S_{pq}\frac{\partial}{\partial \mu} S_{qq}}{S_{qq}^2}$$

$$\frac{\partial S_{qq}}{\partial Q} dQ = \sum_1^N 2(\mu dQ - \frac{1}{N} \sum \mu dQ)(\mu Q - \overline{\mu Q})$$

$$\frac{\partial S_{qq}}{\partial \mu} d\mu = \sum_1^N 2(Q d\mu - \frac{1}{N} \sum Q d\mu)(\mu Q - \overline{\mu Q})$$

$$\frac{\partial S_{pq}}{\partial Q} dQ = \sum_1^N (\mu dQ - \frac{1}{N} \sum \mu dQ)(P - \overline{P})$$

$$\frac{\partial S_{pq}}{\partial \mu} d\mu = \sum_1^N (Q d\mu - \frac{1}{N} \sum Q d\mu)(P - \overline{P})$$

$$\frac{\partial S_{pq}}{\partial P} dP = \sum_1^N (\mu Q dP - \sum \mu Q dP)$$

The errors on the different terms are:

$$\frac{\partial S_{qq}}{\partial Q}\Delta Q = \sum_{1}^{N} 2(\mu\Delta Q + \overline{\mu\Delta Q})(\mu Q - \overline{\mu Q})$$

$$\frac{\partial S_{qq}}{\partial \mu}\Delta \mu = \sum_{1}^{N} 2(Q\Delta \mu + \overline{Q\Delta \mu})(\mu Q - \overline{\mu Q})$$

$$\frac{\partial S_{pq}}{\partial Q}\Delta Q = \sum_{1}^{N} (\mu\Delta Q + \overline{\mu\Delta Q})(P - \overline{P})$$

$$\frac{\partial S_{pq}}{\partial \mu}\Delta \mu = \sum_{1}^{N} (Q\Delta \mu - \overline{Q\Delta \mu})(P - \overline{P})$$

$$\frac{\partial S_{pq}}{\partial P}\Delta P = \sum_{1}^{N} (\mu Q\Delta P + \overline{\mu Q\Delta P})$$

The relative error on A is :

$$\frac{\Delta A}{A} = \sum_{1}^{N} \left[\begin{array}{l} \dfrac{\mu Q\Delta P + \mu Q\Delta P}{S_{pq}} + \\ \dfrac{(\mu\Delta Q + \overline{\mu\Delta Q})(P - \overline{P})}{S_{pq}} + \dfrac{2(\mu\Delta Q + \overline{\mu\Delta Q})(\mu Q - \overline{\mu Q})}{S_{qq}} + \\ \dfrac{(Q\Delta \mu - \overline{Q\Delta \mu})(P - \overline{P})}{S_{pq}} + \dfrac{2(\mu\Delta Q + \overline{\mu\Delta Q})(\mu Q - \overline{\mu Q})}{S_{qq}} \end{array} \right]$$

Error induced by the transverse permeability evaluation

$$K = \left(\frac{1}{A_o} - \frac{1}{A_m}\right)\cdot\frac{e}{S} \qquad \Rightarrow \qquad \frac{\Delta K}{K} = \frac{\Delta\left(\frac{1}{A_o} - \frac{1}{A_m}\right)}{\left(\frac{1}{A_o} - \frac{1}{A_m}\right)} + \frac{\Delta e}{e}$$

S is the cross section area of the flow. It is supposed constant and well define.

$$\frac{\Delta\left(\frac{1}{A_o} - \frac{1}{A_m}\right)}{\left(\frac{1}{A_o} - \frac{1}{A_m}\right)} = \frac{A_m}{A_m - A_o}\cdot\frac{\Delta A_o}{A_o} + \frac{A_o}{A_m - A_o}\cdot\frac{\Delta A_m}{A_m}$$

We can notice here that the larger the difference between regression results, the smaller the made error.

Finally, the uncertainty range on the permeability is:

$$\boxed{\frac{\Delta K}{K} = \frac{A_m}{A_m - A_o} \cdot \frac{\Delta A_o}{A_o} + \frac{A_0}{A_m - A_0} \cdot \frac{\Delta A_m}{A_m} + \frac{\Delta e}{e}}$$

Error induce by the in-plane permeability evaluation

$$K = \left(\frac{1}{A_m}\right) \cdot \frac{ls}{L \cdot e} \qquad \Rightarrow \qquad \boxed{\frac{\Delta K}{K} = \frac{\Delta A_m}{A_m} + \frac{\Delta e}{e}}$$

ANNEXE II

Felt S-1

Direction	Porosity	Permeability μm^2	Relative Error	Exponential fitting μm^2	Kozeny–Carman fitting μm^2
Thickness	0.55	8.00	62.7%	$0.188 \cdot 10^{3.78\varepsilon}$	$\frac{8.6 \cdot \varepsilon^3}{(1-\varepsilon)^2}$
	0.52	4.86	38.1%		
	0.47	3.06	29.3%		
	0.45	2.46	26.0%		
	0.43	2.17	26.4%		
	0.41	1.80	21.4%		
	0.40	1.64	20.9%		
	0.39	1.41	18.3%		
	0.36	1.10	17.4%		
	0.35	0.89	15.5%		
	0.34	0.77	13.9%		
	0.32	0.65	13.2%		
	0.54	10.76	67.7%		
	0.51	4.84	30.3%		
	0.48	3.91	24.5%		
	0.45	3.11	22.0%		
	0.43	2.50	19.2%		
	0.40	1.91	15.9%		
	0.39	1.58	14.5%		
	0.37	1.22	12.4%		
M.D. and C.D.	0.63	55.33	4.0%	$0.167 \cdot 10^{4.68\varepsilon}$	$\frac{24 \cdot \varepsilon^3}{(1-\varepsilon)^2}$
	0.61	41.73	3.1%		
	0.57	26.41	4.8%		
	0.56	22.43	5.6%		
	0.55	19.22	3.1%		
	0.53	14.04	3.9%		
	0.48	8.64	9.6%		
	0.43	5.03	10.6%		
	0.41	3.78	3.7%		

Felt S-2

Direction	Porosity	Permeability μm^2	Relative Error	Exponential fitting μm^2	Kozeny–Carman fitting μm^2
Thickness	0.54	4.41	32.4%	$0.39 \cdot e^{2.10\varepsilon}$	$\frac{13.4 \cdot \varepsilon^3}{(1-\varepsilon)^2}$
	0.48	4.57	36.1%		
	0.42	3.05	28.5%		
	0.38	2.77	28.2%		
	0.33	1.52	17.1%		
	0.44	3.24	28.6%		
	0.39	2.94	28.3%		
	0.33	1.93	21.7%		
M.D.	0.54	16.29	5.7%	$0.30 \cdot e^{3.81\varepsilon}$	$\frac{43 \cdot \varepsilon^3}{(1-\varepsilon)^2}$
	0.51	12.70	5.2%		
	0.43	7.13	4.9%		
	0.37	3.27	4.7%		
	0.35	2.54	5.0%		
C.D.	0.50	15.56	5.8%	$0.10 \cdot e^{4.14\varepsilon}$	$\frac{22.6 \cdot \varepsilon^3}{(1-\varepsilon)^2}$
	0.46	13.30	5.4%		
	0.39	7.35	5.1%		
	0.33	4.08	5.1%		
	0.28	2.79	4.6%		
45°/M.D.	0.53	16.83	5.5%	$0.1186 \cdot e^{4.16\varepsilon}$	$\frac{30.66 \cdot \varepsilon^3}{(1-\varepsilon)^2}$
	0.49	13.08	5.4%		
	0.41	7.44	5.4%		
	0.36	3.75	4.9%		
	0.31	1.97	4.8%		

Felt S-3

Direction	Porosity	Permeability μm^2	Relative Error	Exponential fitting μm^2	Kozeny-Carman fitting μm^2
Thickeness	0.41	1.90	27.4%	$0.53 \cdot e^{4.37\varepsilon}$	$\frac{10 \cdot \varepsilon^3}{(1-\varepsilon)^2}$
	0.38	1.67	23.6%		
	0.34	0.68	11.4%		
	0.27	0.27	7.5%		
	0.46	4.15	50.6%		
	0.43	2.85	38.7%		
	0.37	1.42	22.6%		
	0.33	0.70	13.8%		
	0.29	0.31	8.2%		
In-plane	0.49	6.66	4.4%	$0.227 \cdot e^{4.28\varepsilon}$	$\frac{16.7 \cdot \varepsilon^3}{(1-\varepsilon)^2}$
	0.44	4.65	4.6%		
	0.40	3.20	4.5%		
	0.36	2.09	4.5%		
	0.32	1.16	4.8%		
	0.28	0.61	4.9%		
	0.44	4.57	4.8%		
	0.35	1.96	4.9%		
	0.31	1.01	4.7%		
	0.27	0.60	5.6%		

Transcription of Discussion

PERMEABILITY MEASUREMENTS OF PRESS FELTS

X. Thibault, Y. Chave, J-M. Serra-Tosio, J-F. Bloch

Laboratoire Génie des Procédés Papetiers

Shri Ramaswamy University of Minnesota

Where did you get the surface area and tortuosity numbers to calculate the Kozeny–Carman figures?

Xavier Thibault

We did not measure these numbers. We considered the first term A_c of the equation of Kozeny–Carman (Eq. i) was not strain dependant as we were not able to measure the Kozeny–Carman parameter ($k_o\tau^2$).

$$A = \frac{1}{k_o \tau^2 S_m^2}$$ Equation i: Parameter of the Kozeny–Carman model

Shri Ramaswamy

So how do you calculate?

Xavier Thibault

A_c was considered as a parameter. The value of this parameter is obtained by fitting the experimental results with the model.

Shri Ramaswamy

So the slope of that equation covered the rest of the parameters.

Xavier Thibault

Yes, nevertheless this parameter influences more the ordinate at the origin than the slope.

Bill Sampson Department of Paper Science, UMIST

The very feature that you are looking at is the anisotropy of the flow in the felt is due to the anisotropy of the material, but the Kozeny–Carman model just used porosity which is an orthotropic property of the material, and what changes is the organization of that porosity in different direction. I think that is unrealistic to expect Kozeny–Carman or any other model which uses porosity as a variable to fit your data.

Xavier Thibault

First of all, we wanted to test the efficiency of the Kozeny–Carman model. Furthermore, the tortuosity may be considered as a directional property. Our results showed us that the Kozeny–Carman relationship is not adapted to take into account the compression dependance of felt permeability. This conclusion reinforces your point of view if we are considering the tortuosity as a scalar.

Next, we used the porosity not as a geometrical variable, but as a strain variable (porosity is strain dependent) as we have the following relation (Equation ii) between the felt strain and the porosity ε considering felt compression.

$$\varepsilon = \frac{1 - w}{p_f e}$$

Equation ii: Relation between felt thickness and its porosity.

with **w**, the felt basis weight, $\mathbf{p_f}$, the fibers and yarns density, **e**, the felt thickness.

Thus, we have presented the results as a function of porosity. However to illustrate your comment we present here the analyse of the porosity evolution through the felt S-1 thickness (Figure 1).

This curve was calculated using the reconstructed volume slice of our X-ray microtomography measurements. The porosity is represented versus the slice number (a slice each 6.6 microns). The curve is for the felt S-1 with no strain. As the curve starts the porosity is high because there are few fibers

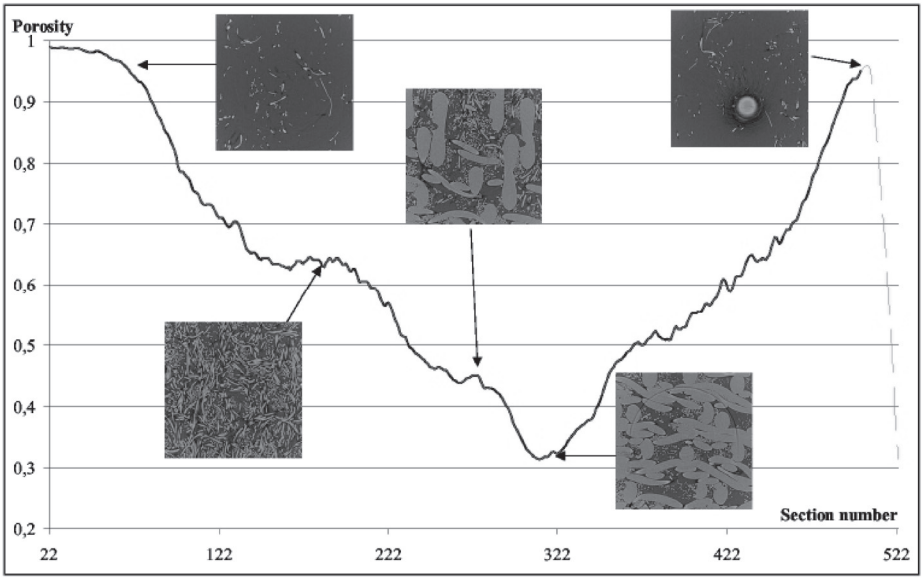

Figure 1 Porosity evolution towards felt thickness

then penetrating inside the batt the porosity decreased rapidly and the minimum is reached inside the base. This porosity behaviour may be taken in to account when modeling the felt transverse permeability.

Gary Baum Institute of Paper Science & Technology

Is it your intention to use this device to design improved felts?

Xavier Thibault

First of all, we have to relate the felt structure to the physical properties.

X-ray measurements have been conducted on the felt using the absorbtion contrast technique (Thibault, X., J.-F. Bloch, and E. Boller, *Tissue structure characterised by synchrotron microtomography*. APPITA, 2001). Example of the 3-D construction results are shown just below for S-1 and S-3 samples (Figures 2 and 3). Pictures illustrate the felt compression. The left image represents the felt with no strain. The right one is a strained state.

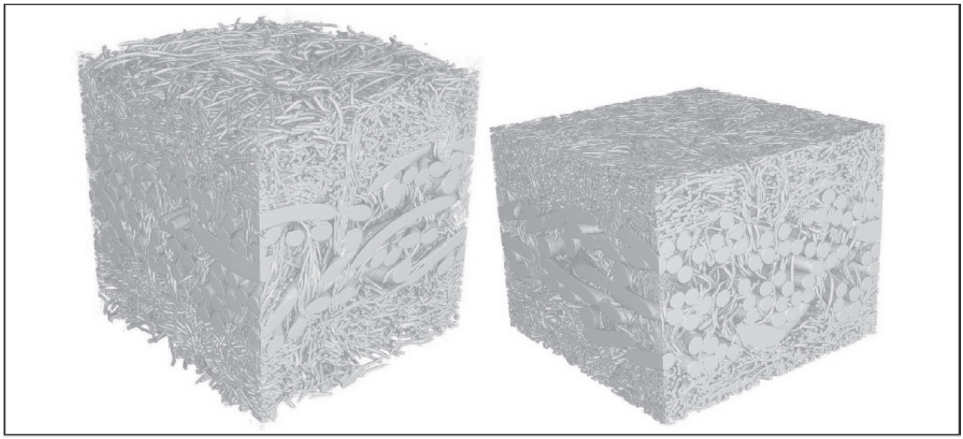

Figure 2 Felt S-1 reconstruction by X-ray computed microtomography

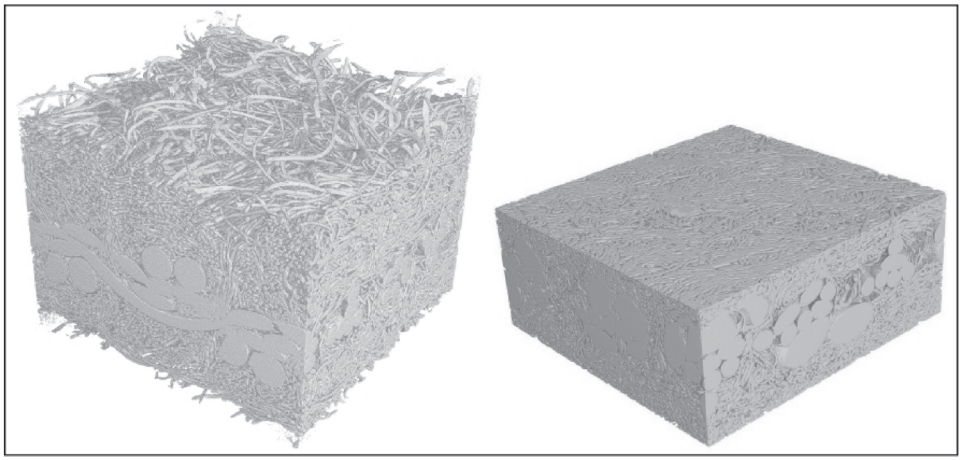

Figure 3 Felt S-3 reconstruction by X-ray computed microtomography

X-ray computed microtomography is a powerful tool for the investigation of porous media structure. This technique allows the fine description of the fibrous structure.